Localized excitons and their decay into electron and hole centres in $PbWO_4$ single crystals grown by the Bridgman method

2007 J. Phys.: Condens. Matter 19 306202

(http://iopscience.iop.org/0953-8984/19/30/306202)

IOP PUBLISHING JOURNAL OF PHYSICS: CONDENSED MATTER

J. Phys.: Condens. Matter **19** (2007) 306202 (14pp) doi:10.1088/0953-8984/19/30/306202

Localized excitons and their decay into electron and hole centres in $PbWO_4$ single crystals grown by the Bridgman method

A Krasnikov[1], V Laguta[2,3], M Nikl[3] and S Zazubovich[1]

[1] Institute of Physics, University of Tartu, Riia 142, 51014 Tartu, Estonia
[2] Institute for Problems of Material Sciences, National Academy of Sciences of Ukraine, Krjijanovskogo 3, 03142, Kiev, Ukraine
[3] Institute of Physics AS CR, Cukrovarnicka 10, 162 53 Prague, Czech Republic

E-mail: svet@fi.tartu.ee (A Krasnikov)

Received 27 January 2007, in final form 29 May 2007
Published 3 July 2007
Online at stacks.iop.org/JPhysCM/19/306202

Abstract

Lead tungstate crystals grown by the Bridgman method are oxygen deficient. Therefore they are suitable objects for the detailed study of various oxygen vacancy-related defects. The processes of luminescence and photo-thermally stimulated defect creation were studied at 80–350 K under selective UV irradiation in the 5.0–3.5 eV energy range for as-grown and 600 °C air annealed $PbWO_4$ crystals (grown in both cases by the Bridgman method). The creation of defects reveals itself in the appearance of thermally stimulated luminescence (TSL) peaks and electron spin resonance signals. Dependences of the TSL peak intensity on the irradiation energy, temperature and duration were investigated. In the crystals studied the observed characteristics are explained by the presence of excitons localized at oxygen-deficient anion complexes of different types (WO_3, WO_2, WO) and the photo-thermally stimulated decay of these excitons into electron and hole centres. The origin of these centres and their creation processes are discussed.

(Some figures in this article are in colour only in the electronic version)

1. Introduction

Luminescence of lead tungstate became a subject of renewed interest about 13 years ago when this material was chosen for use in high-energy physics detectors [1]. The results obtained during the study of its scintillation characteristics and material optimization were reviewed in [2, 3]. In the luminescence spectrum of $PbWO_4$ crystals, the blue emission, two types of green emission and two types of red emission have been observed. The blue (B) emission arises from the radiative decay of the self-trapped and localized excitons of the $(WO_4)^{2-}$ type [4]. In undoped crystals, the low-temperature green G(I) emission was ascribed to excitons of the type $(WO_4)^{2-}$ localized in the lead-deficient crystal regions [3, 5, 6]. The green G(II)

emission, appearing in some crystals at $T > 150$ K, was ascribed to the oxygen-deficient anion complexes in the form of WO_3 [5, 7, 8]. In [9] it was shown that this emission appears in tunnelling recombination processes. The red emission reported in [1, 10] was ascribed in [11] to lead vacancies V_{Pb} and to associates of V_{Pb} with trivalent rare-earth ions A^{3+}.

In [12], the photo-thermally stimulated decay of the exciton- and defect-related states was revealed under UV irradiation. Further investigations [4, 6, 7, 11–16] showed that systematic study of the optical creation of defects at different temperatures under monochromatic UV irradiation with different energies followed by detection of the created defects using a thermally stimulated luminescence (TSL) method is a very sensitive and powerful investigation tool. It gives important information regarding (i) the origin of exciton states; (ii) the origin of defects, responsible for the photo- and thermally stimulated luminescence; (iii) the processes occurring in the excited state of luminescence centres and at the radiative recombination of charge carriers. For the first time, various localized exciton states were identified in [4] and their decay into stable defects was found. It was also shown that oxygen and lead vacancies play an important role in the trapping of electrons and holes, respectively, and in the optically and thermally stimulated recombination processes.

Lead tungstate crystals grown by the Bridgman method are oxygen deficient. According to [17], in the as-grown samples oxygen-deficient anion complexes of the WO_2 and WO type prevail over WO_3-type complexes. The annealing of these samples in both oxygen-rich (air) and inert (Ar) atmospheres around 600 °C results in the transformation of the WO_2 and WO complexes into complexes of the WO_3 type. For this reason the mentioned crystals are the most suitable ones for the study of various oxygen vacancy-related phenomena. Some characteristics of these crystals have been reported in [4, 5, 7, 9, 14, 18].

In the present work the photo-thermally stimulated decay of exciton states was studied at 80–350 K under selective UV irradiation in the 5.0–3.5 eV energy range for as-grown and 600 °C air annealed $PbWO_4$ crystals (grown in both cases by the Bridgman method) [17]. Defect creation reveals itself in the appearance of TSL peaks and electron spin resonance (ESR) signals. Dependences of each TSL peak intensity on the irradiation energy (E_{irr}), irradiation temperature (T_{irr}) and irradiation duration (t_{irr}) were measured. The aim of the work was to clarify the influence of different types of oxygen vacancies (WO_3, WO_2, WO) on the exciton states and their decay processes, and to obtain information on the origin of the defects created during the nonradiative decay of excitons.

2. Experimental details

The sample in the nitrogen cryostat was located at a position which allowed us to detect the luminescence from its excited front surface. This crystal position allowed us to minimize the effects arising from strong absorption of excitation light in the absorption region of the host material. Emission and excitation spectra were measured in the 80–300 K temperature range under excitation with a deuterium DDS-400 lamp in a set-up consisting of two monochromators. The amplified luminescence signal was detected by a suitable photomultiplier (FEU-39 or FEU-79). The spectra were corrected for the spectral distribution of the excitation light, the transmission and dispersion of the monochromators and the spectral sensitivity of the detectors.

Thermally stimulated luminescence glow curves $I_{TSL}(T)$ were measured in the same set-up with a constant heating rate of 0.2 K s^{-1} for the crystal after UV irradiation by the DDS-400 lamp through a monochromator for 15 min, the spectral width of the slit being about 5 nm. TSL intensity was detected by FEU-39 (for the green emission) or FEU-79 (for the red emission). All the TSL glow curves shown in this paper were measured for the green (2.5 eV) emission.

Table 1. Maximum position (E_{em}^{max}) and full width at half maximum (FWHM) of the B emission band, maximum position of the exciton band in the excitation spectrum of the B emission (E_{exc}), the emission intensity ratios under excitation at 4.1 and 4.3 eV obtained at different E_{em} and the intensity ratio of the B, G(I) and R emission bands obtained at 80 K.

Crystal	E_{em}^{max} (eV)	FWHM (eV)	E_{exc} (eV)	∼4.1/4.3 ratio	B:G(I):R
As-grown	2.72–2.76	0.63	4.10–4.15	1.43–3.6	210:27:10
Ann. 600 °C in air	2.78	0.64	4.15	1.88–1.82	210:28:7

The irradiation energy (E_{irr}) dependence of the TSL peak intensity (the creation spectrum) was measured for all TSL peaks. The T_{irr} dependence of the TSL peak intensity was also measured to obtain the activation energies (E_a) for the creation of TSL peaks. To avoid the irradiation-induced destruction of the centres responsible for a TSL peak, the irradiation temperature was at least 50 K lower than the temperature of the TSL peak maximum.

For the ESR study, oriented samples ($2.5 \times 2.5 \times 6$ mm^3) carefully cut along the (001), (100) and (110) planes were used. ESR measurements were performed at 9.22 GHz and at temperatures from 4 K up to 100 K using an Oxford Instruments ESR 9 cryostat [18]. A high-pressure mercury arc lamp with optical filters was used for the UV irradiation of the sample. Thermal stability of the light-induced paramagnetic centres was studied by the method of isochronal annealing. After irradiation at low temperature (usually 60–160 K), the sample was heated at a rate of $\approx$1 K s^{-1} up to a given temperature T_{ann}, held at that temperature for 2–3 min, and then quickly cooled (at a rate of $\approx$4 K s^{-1}) to the temperature where the ESR spectrum was measured.

3. Experimental results

3.1. Luminescence characteristics

At 80 K, the emission spectrum of both the as-grown and the annealed samples consists of the well-known intense blue (B) band, weak green (G(I)) band and weak red (R) bands (see, e.g., [3–6, 11]). The G(I) band peaks at 2.4 eV (FWHM = 0.56 eV) and is excited around 3.92 eV. The R band is located at 1.55 eV and is excited in the bands with maxima at 4.0 and 3.55 eV. Unlike the B, G(I) and R bands, whose relative intensities are similar in both samples studied, G(II) emission appears just as a result of the annealing. The G(II) band is located at 2.5 eV (FWHM = 0.55 eV). At 220 K, this emission is most effectively excited around 4.08 eV. It is also excited in the band-to-band and in the defect-related absorption region [5, 7, 9].

Characteristics of the B emission differ noticeably in the two samples studied (table 1). In the as-grown crystal, both the B emission band and the exciton band in the excitation spectrum of the B emission are located at lower energies as compared with other $PbWO_4$ crystals studied [4]. The B emission spectrum depends on the excitation energy (figure 1(a)) and the excitation spectrum of the B emission depends on the emission energy (figure 1(b)) which points to a complex structure of these spectra [19]. In the annealed crystal, the above-mentioned dependences are much weaker, the emission band is located at 2.78 eV, and the excitation spectrum is similar to curve 3 in figure 1(b).

3.2. Creation of electron and hole centres

3.2.1. TSL glow curves (the I_{TSL} (T) dependences). TSL glow curves were measured after irradiation of the crystals at different temperatures T_{irr} (varying from 80 to 295 K) and with

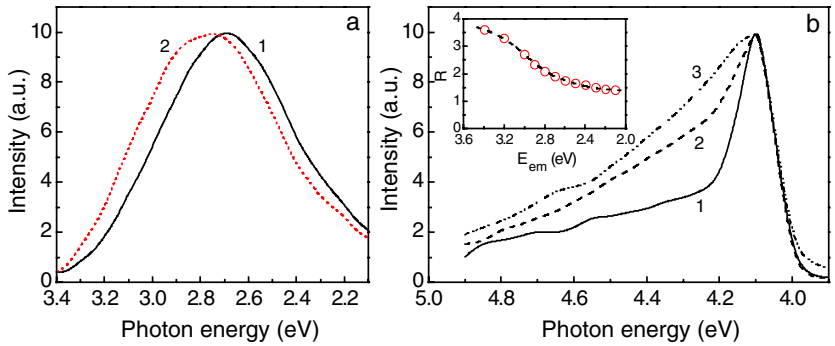

Figure 1. (a) Emission and (b) excitation spectra measured at 80 K for the B emission of as-grown $PbWO_4$ Bridgman crystal under $E_{exc} = 4.4$ eV ((a), curve 1) and $E_{exc} = 4.1$ eV ((a), curve 2), and for $E_{em} = 3.4$ eV ((b), curve 1), $E_{em} = 2.8$ eV (b), curve 2) and 2.6 eV ((b), curve 3). In the inset: ratios (R) of the B emission intensities at $E_{exc} = 4.1$ and 4.3 eV obtained at different E_{em}.

Table 2. TSL peak positions in $PbWO_4$ Bridgman crystals under different irradiation conditions (the most intense peaks are shown in bold).

		TSL peak position (K)	
T_{irr} (K)	E_{irr} (eV)	In the annealed sample	In the as-grown sample
80	4.90–4.30	**105–107, 173–175**, 195–200, 226, ∼238, 280	**110**, 132, 195, 226
	4.17–4.12	105–107, 173–175, 200, **213**, ∼238, 280	110 200, **233**
	4.05–3.80	105–107, 173–175, ∼200, ∼**238**, 280	
133	4.90–4.30	**166**, ∼190, ∼212, ∼220	183, 198, **228**
	4.17–4.10	172–175, **202–205**, 226–232	183, 200, **230**, 305, 342
	4.05–3.75	172–175, 192, 212, **226–238**	183, 200, **232**, 305, 342
152	4.8	**185–190**, 226	200, **228**
	4.20–4.07	**205**, 232, 280, 305	200, **230**, 305, 342
	<4.05	205, **232–236**, 305	200, **232**, 305, 342

different energies E_{irr} (varying from 5.0 to 3.5 eV). The irradiation duration t_{irr} varied from 0.5 to 90 min. At $T < 295$ K, the electron recombination G(II) emission band is observed in the TSL spectrum, but at $T > 295$ K, the R emission prevails. The TSL peak positions are presented in tables 2 and 3. The dependences of the TSL intensity (I_{TSL}) on E_{irr}, T_{irr} and t_{irr} were measured. The following main features were observed:

(i) A comparison of maximum intensities, taken from the TSL peaks creation spectra, indicates that the total TSL intensity in the annealed crystal is several times larger than in the as-grown one. The TSL glow curves, measured for these crystals after irradiation at the same conditions in the exciton region (at about 4.0–4.1 eV), are strongly different: in the as-grown crystal, the complex ≈230 K peak dominates, while in the annealed crystal, the ≈205 K peak is more intense (figure 2). After irradiation in the defect-related region (around 3.9 eV), the TSL peak near 230 K dominates in both crystals. In the annealed crystal irradiated at 152 K the intensity of the 205 K peak is about four times larger, that of the 230 K peak is about 1.4 times smaller, and that of the ≈305 K and 340 ± 5 K peaks is about three times smaller, compared with the as-grown crystal.

(ii) The TSL glow curves are strongly different after irradiation of the crystal in the band-to-band (figure 3, curve 1), exciton (curve 2) and defect-related (curve 3) absorption regions. At $E_{irr} > 4.3$ eV, the TSL curve structure is practically independent of E_{irr}.

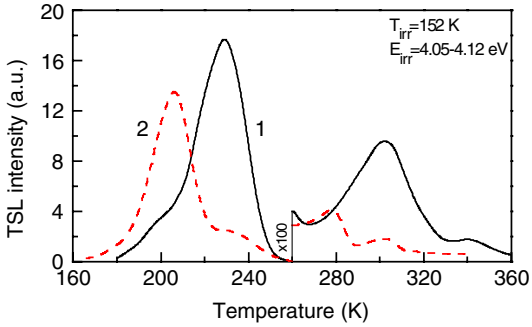

Figure 2. The TSL glow curves measured for the as-grown $PbWO_4$ Bridgman crystals (curve 1) and those annealed at 600 °C for 2 h in air (curve 2) after irradiation in the exciton region at $T_{irr} = 152$ K.

Table 3. Creation spectrum maximum E_{max}, trap depth E_t and the activation energy E_a for the TSL peak creation obtained for different TSL peaks.

	The as-grown crystal					
TSL peak	183 K	200 K	∼230 K	305 K	342 K	
E_{max} (eV) at 133 K	4.10		4.09			
E_{max} (eV) at 140 K	4.09	4.09	4.07	4.02		
E_{max} (eV) at 152 K		4.06	4.04	4.02	4.04	
E_{max} at 221 K				3.91	3.93	
E_t (eV)			0.57	0.71		
E_a (eV)		∼0.20	0.27	0.16	0.17	
	The annealed crystal					
TSL peak	172 K	192 K	205 K	∼230 K	280 K	305 K
E_{max} (eV) at 80 K	4.15	4.15	4.15	4.05	4.17	
E_{max} (eV) at 133 K	4.13		4.11	4.04		
E_{max} (eV) at 140 K		4.13	4.11	4.03	4.17	∼4.08
E_{max} (eV) at 146 K			4.11	4.03		∼4.07
E_{max} (eV) at 152 K			4.10	4.02	4.17	4.10–4.02
E_t (eV)	0.23	0.34	0.50	0.56		
E_a (eV)	0.04	0.04	0.18	0.29	0.08	0.17

(iii) Different TSL peaks appear after irradiation of the annealed sample at $T_{irr} = 80$ K and $T_{irr} > 130$ K (table 2).

(iv) The TSL glow curve depends on the duration of the irradiation (figure 4). The $I_{TSL}(T_{irr})$ curves depend on the irradiation energy (figure 5). Under irradiation in the exciton and defect-related absorption regions, the dependences of the TSL peak intensity on t_{irr} are different for different peaks. This means that they arise from different centres.

The trap depths E_t, corresponding to the main TSL peaks, were determined by the partial cleaning method from the $\ln I_{TSL}(1/T)$ dependences after heating the sample up to selected temperatures T_{stop}. Due to the complex structure of some TSL peaks, the E_t values depend on T_{stop} (figure 6). The values of E_t obtained for different TSL peaks are shown in table 3.

3.2.2. TSL peak creation spectra (the $I_{TSL}(E_{irr})$ dependences). *Under irradiation of the annealed sample at* $T_{irr} = 80$ K, the TSL peaks located at about 106, 174, 200, 213 and 280 K

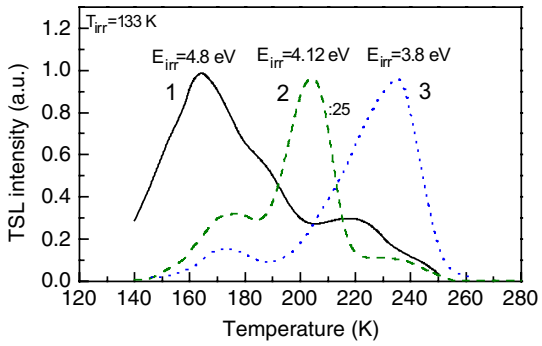

Figure 3. The TSL glow curves (normalized) measured for the $PbWO_4$ Bridgman crystal annealed at 600 °C for 2 h in air after irradiation at 133 K in the band-to-band (curve 1), exciton (curve 2, decreased ≈25 times with respect to the curves 1 and 3) and defect-related (curve 3) energy regions.

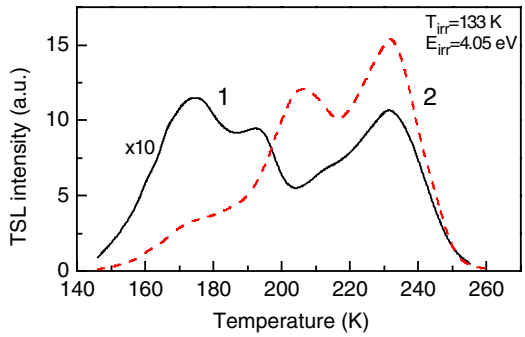

Figure 4. The TSL glow curves measured for the $PbWO_4$ Bridgman crystal annealed at 600 °C for 2 h in air after irradiation at 133 K for 5 min (curve 1, increased 10 times) and 20 min (curve 2). $E_{irr} = 4.05$ eV.

are mainly created in the band-to-band and exciton absorption regions where their creation efficiencies are comparable. In the exciton region, these peaks are created in a narrow band with a maximum at 4.15–4.17 eV. The 238 K peak is efficiently created also in the defect-related region.

Under irradiation at $T_{irr} > 130$ K, the TSL peaks are selectively created mainly in the exciton absorption region (figure 7). The creation spectra are relatively narrow bands (FWHM ≈ 0.15 eV) located in the 4.02–4.11 eV energy range. Their positions are different for different TSL peaks and also depend on T_{irr} (see also table 3). At $E_{irr} > 4.3$ eV, their creation efficiency is relatively small and practically independent of the irradiation energy. A weak 280 K peak is created around 4.17 eV and in the band-to-band absorption region (figure 7(b), curve 3).

3.2.3. Activation energies for TSL peak creation. From the $I_{TSL}^{max}(1/T_{irr})$ dependences, where I_{TSL}^{max} is the TSL intensity at the maximum of the TSL peak creation spectra measured at different T_{irr}, the activation energies E_a were calculated for each TSL peak creation. Activation energies E_a for the 170–190 K, 205 K and ≈230 K peak creations are about 0.04, 0.19 and 0.28 eV, respectively. The peaks at 305 K and near 340 K are created with $E_a \approx 0.17$ eV (table 3). It is interesting to note that the linear $\ln I_{TSL}^{max}(1/T_{irr})$ dependence is only observed for these peaks at

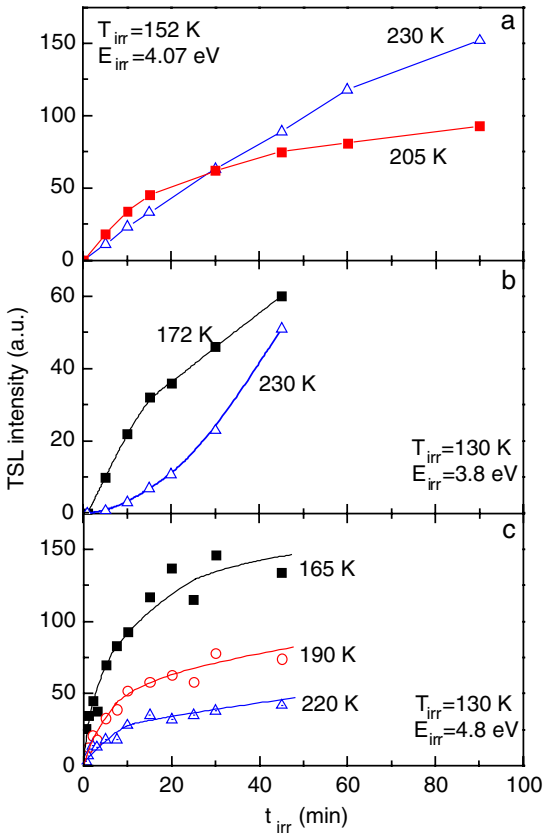

Figure 5. Dependences of various TSL peak intensities on the irradiation duration (T_{irr}) measured for the $PbWO_4$ Bridgman crystal annealed at 600 °C for 2 h in air after irradiation in the exciton (a), defect-related (b) and band-to-band (c) energy regions.

$T_{irr} < 165$ K. At higher T_{irr}, the TSL intensity reaches saturation and then decreases (figure 8). At room temperature no TSL peaks are optically created in the annealed crystal. The value of $E_a \approx 0.07$–0.08 eV characteristic for the self-trapped exciton (STE) decay [4] was obtained for all the TSL peaks under irradiation at 4.4 eV, and for the 280 K peak, also under irradiation in the exciton band. The E_a value for the creation of the 172 and 192 K peaks is about 0.04 eV. In the 80–120 K range, the E_a values for all the created TSL peaks do not exceed 0.04 eV.

Thus, the most effective defect creation takes place under crystal irradiation in the exciton absorption region at $T_{irr} = 165$ K.

3.2.4. Dependences of the TSL intensity on irradiation dose. The dependences of the TSL intensity on the irradiation duration t_{irr} are different for different TSL peaks and depend on the irradiation energy (see, e.g., figure 5). These data surely point to a different origin for centres responsible for different peaks as well as to different kinetics of their creation. For example, under irradiation in the band-to-band transitions region, where free electrons are trapped by the traps existing in the crystal, sublinear $I_{TSL}(t_{irr})$ dependences are observed for all the TSL peaks (figure 5(c)). Similar dose dependences are obtained for the 172 and 192 K peaks under irradiation in the exciton band. For the TSL peaks at ≈205 and 230 K, different

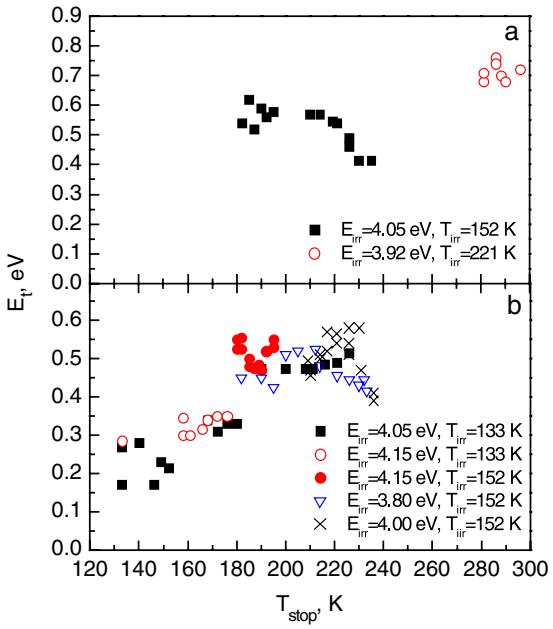

Figure 6. Dependences of the trap depth E_t on T_{stop} obtained at different irradiation conditions for $PbWO_4$ Bridgman crystals: (a) as-grown and (b) annealed at 600 °C for 2 h in air.

dose dependences are observed under excitation in the exciton and in the defect-related regions (see figures 5(a) and (b)).

3.3. ESR characterization

ESR measurements showed that the non-irradiated as-grown samples contain Ce^{3+} ions at a concentration of a few ppm. Another signal with superhyperfine structure is ascribed to $(CrO_4)^{3-}$ (figure 9(a)) and is very similar to that of the $(MoO_4)^{3-}$ centre [18]. The centre of gravity of the $(CrO_4)^{3-}$ spectrum was described by a spin Hamiltonian of tetragonal symmetry for a particle with a spin $S = 1/2$ and g-factors of $g_\parallel = 1.9602(5)$, $g_\perp = 1.9004(5)$, where the indices '$\parallel$' and '$\perp$' mean that the magnetic field is parallel or perpendicular, respectively, to **c** axis of the crystal. As in the case of other unperturbed electronic centres with tetragonal symmetry, e.g. $(WO_4)^{3-}$ and $(MoO_4)^{3-}$, the superhyperfine structure of the ESR line originates from the interaction of a d^1 electron with two sets of four equivalent ^{207}Pb nuclei (for details, see [18]). This unambiguously proves that paramagnetic ion is located at a W lattice site, which is arranged with four oxygen ions in D_{2d} tetrahedral symmetry. Respectively, measured g-factors correspond to the d_z^2 ground orbital state, but are closer in value to the g-factor for a free electron ($g_e = 2.0023$) than the g-factors of the $(WO_4)^{3-}$ and $(MoO_4)^{3-}$ centres, in good agreement with the smaller spin–orbit coupling constant of Cr^{5+} ion ($\lambda \approx 200$–250 cm^{-1}). Therefore, in spite of the fact that hyperfine structure of the ^{53}Cr isotope was not detected, we assigned the observed spectrum to the Cr^{5+} ion in the $(CrO_4)^{3-}$ complex anion.

After illumination by UV light around 330 nm (3.7-4.0 eV) at a temperature of 160–170 K, the ESR spectra of $\{Pb^+–WO_3\}$ [20] and $(MoO_4)^{3-}$ [18] centres are produced (figure 9(b)). The presence of $(MoO_4)^{3-}$ centres in the crystals studied also reveals itself in the appearance of a weak TSL peak at 250 K which becomes evident in the crystal irradiated at 230 K. The ESR

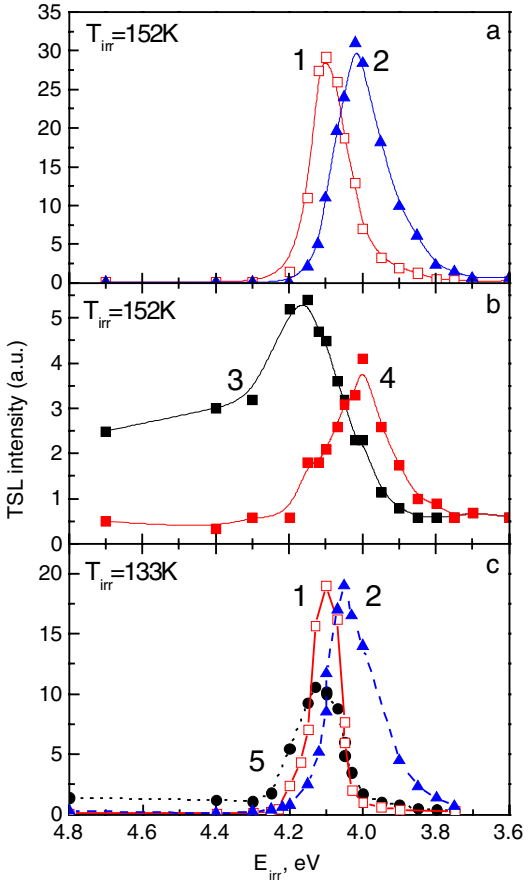

Figure 7. Creation spectra of the TSL peaks located at 205 K (curve 1), 230 K (curve 2), 280 K (curve 3), 305 K (curve 4) and 172–175 K (curve 5) measured for $PbWO_4$ Bridgman crystal annealed in air at 600 °C for 2 h after its irradiation at 152 K (a), (b) and 133 K (c).

intensity of the oxygen-deficient $\{Pb^{+}–WO_3\}$ defects is at least ten times larger than in crystals grown by the Czochralski method and studied earlier in the same set-up [20]. This indicates a much larger concentration of oxygen vacancies in the crystals grown by the Bridgman method. The number of these defects further increases (around 25–30%) in annealed crystals. Heating of the crystals to 180-190 K transforms the $\{Pb^{+}–WO_3\}$ spectrum into other oxygen vacancy-related spectra due to retrapping of the thermally released electrons to deeper traps, namely (WO_3) and possibly (WO_2) group-related electron centres perturbed by a defect at the Pb lattice site (figure 9(c)). Centres of the type of $(WO_3)^{-}–A_{Pb}$ are stable up to 350–370 K (figure 9(d)). They have been described by us previously [21]. The signal designated as 'x' was not identified. However, its behaviour with illumination and temperature annealing is similar to that of $(MoO_4)^{3-}$ centres.

Figure 10 shows the changes in the ESR intensities of different centres measured after isochronal annealing of the illuminated sample at a given temperature. One can notice a marked decrease in the concentration of $(MoO_4)^{3-}$ and $(CrO_4)^{3-}$ electron centres after heating of the sample to 200–220 K, in spite of the fact that they are thermally stable at these temperatures. These data indicate that hole centres are also thermally destroyed in this temperature range.

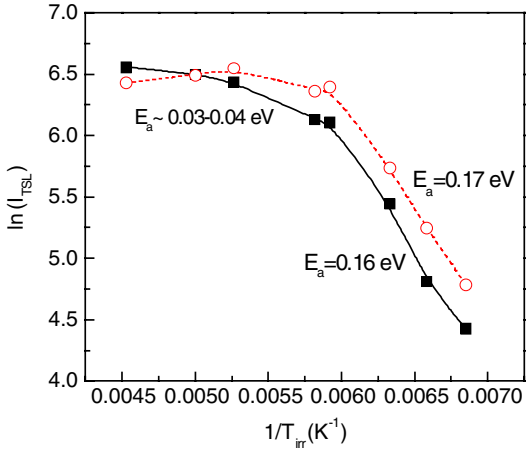

Figure 8. Dependences of the TSL peak intensity on the irradiation temperature obtained for the 305 K (curve 1) and ≈340 K (curve 2) peaks in the as-grown crystal after irradiation in their creation spectra maxima.

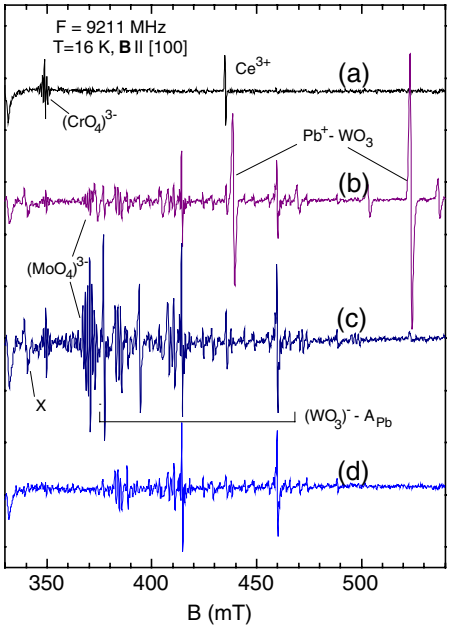

Figure 9. ESR spectra of the non-irradiated (a) and irradiated (3.7–4.0 eV) at 160 K (b) as-grown $PbWO_4$ Bridgman crystal. The spectra (c) and (d) were measured after heating of the irradiated sample up to 190 and 300 K, respectively. In the crystal annealed at 600 °C for 2 h in air, the ESR spectral intensity of the WO_3^--related centres increases by about 25–30%.

Indeed, the observed decrease in the number of $(CrO_4)^{3-}$ electron centres around 200–220 K might be caused just by their recombination with thermally released holes.

It is worth noting that after UV irradiation the concentration of $(CrO_4)^{3-}$ centres markedly decreases (compare the spectra (a) and (b) in figure 9). The most probable reason is their

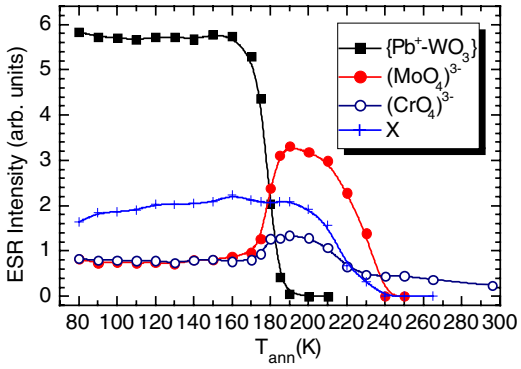

Figure 10. Temperature dependences of the ESR signal intensities of the electron $\{Pb^{+}–WO_3\}$, $(MoO_4)^{3-}$, $(CrO4)^{3-}$ and unidentified 'x' centres measured at 16 K for the air annealed $PbWO_4$ Bridgman crystal after its irradiation at 80 K in the 3.7–4.0 eV energy range and subsequent isochronal annealing at different T_{ann}. A shift in temperature where $\{Pb^{+}–WO_3\}$ and $(MoO_4)^{3-}$ centres become destroyed as compared with the TSL data (see figure 2, curve 2 and [4]), is caused by the different heating conditions used in the ESR and TSL experiments.

direct ionization by light with an energy lower than the band-gap. The recombination of holes released during localized exciton decay with $(CrO_4)^{3-}$ centres is not excluded either.

4. Discussion

The complexity of the luminescence characteristics of the crystals studied points to the presence of a large number of various intrinsic defects. The data obtained for the as-grown sample indicate that the B emission band and the exciton band in the excitation spectrum of the B emission may be considered as a superposition of many separate bands arising from different exciton states (see also [4]). This is also true for other $PbWO_4$ crystals and can explain the different positions of the B emission band and its lowest-energy exciton-related excitation band, the different temperature dependences of the B emission intensity and the different degrees of polarization observed for the B emission in different works.

The studies [4] have shown that *under irradiation of a crystal in the exciton absorption region*, creation spectra of different TSL peaks are narrow bands, whose positions are different for different TSL peaks. The conclusion was made that different electron centres are selectively created by the decay of the excitons of the type of $(WO_4)^{2-}$ localized near different defects (e.g. trivalent rare-earth ions, oxygen vacancies of the type of WO_3, $(MoO_4)^{2-}$ groups, etc). Strongly selective creation of the TSL peaks, as well as the data on the decay kinetics of the G(II) recombination luminescence obtained in [9], indicate that free electrons are not released at the localized exciton decay. Similar creation spectra were obtained in [13, 14, 16] in the systematic study of many undoped and Mo-doped $PbWO_4$ Czochralski crystals. The TSL peak creation spectra obtained in the present paper also point to the presence of strongly overlapping narrow exciton bands of different origin. Besides the localized exciton decay, electron centres can also be created due to the trapping of free electrons released during STE decay with $E_a \approx 0.08$ eV (e.g. the TSL peak at 280 K) as well as due to the charge-transfer processes in close defect pairs taking place with $E_a < 0.04$ eV. However, at $T_{irr} > 130$ K, the efficiency of defect creation at the localized exciton decay strongly prevails over the other processes mentioned above.

From comparison of the TSL glow curves, measured after irradiation at $T_{irr} = 80$ K and at $T_{irr} > 130$ K, as well as in the band-to-band and in the exciton absorption region, it is evident

that different TSL peaks are created during the trapping of free electrons at the traps existing in the crystal lattice, and at the decay of localized excitons, occurring without release of free electrons.

As mentioned in the introduction, the main difference between the as-grown and the annealed $PbWO_4$ Bridgman samples consists of the relative concentration of oxygen vacancies of different types. According to [17], the as-grown $PbWO_4$ Bridgman samples contain many oxygen-deficient anion complexes of the WO_2 and WO type, and their annealing in air around 600 °C results in the transformation of these complexes into complexes of the WO_3 type. Different creation spectra, dose dependences, trap depths E_t and activation energies E_a obtained for different TSL peaks indicate that they arise from the centres of different origin. Comparison of the data obtained in the present paper with those reported in [17] allows us to assume that the TSL peaks at 170–205 K, dominating in the annealed sample, can be connected with the oxygen-deficient WO_3 group-related electron centres. The centres responsible for the 172 and 192 K peaks are probably produced due to the electron transfer from the excited $(WO_4)^{2-}$ groups to closely located defects, i.e. due to the processes which take place at $T < 160$ K with the same activation energy of 0.02–0.04 eV and lead to the thermal quenching of the B emission [19]. The 200–205 K peak appears as a result of thermal destruction of $\{Pb^+–WO_3\}$ centres. Indeed, the corresponding trap depth is the same as that obtained for these centres in [20]. The annealing-induced increase of its intensity is consistent with the increased number of $\{Pb^+–WO_3\}$ centres detected by the ESR method in the annealed sample. The high-temperature shift of this peak in our measurements as compared with [20] and the ESR characteristics reported here can be explained by unequal crystal heating conditions in different cryostats (for more details, see [4]).

In [4] it was concluded, that one of the effective mechanisms of creation of $\{Pb^+–WO_3\}$ centres is the photo-thermally stimulated decay of the $(WO_4)^{2-}$-type exciton localized near an oxygen vacancy of the WO_3 type and subsequent trapping of its electron component by a Pb^{2+} ion located close to oxygen-vacant WO_3 group. This process takes place without release of free electrons into the conduction band. This is also supported by the fact that the number of optically created $\{Pb^+–WO_3\}$ centres, which are directly detected by ESR, strongly increases as the irradiation temperature increases from 60 K to $T > 150$ K, where the localized excitons are being effectively destroyed. Analogous processes could also be responsible for the appearance of other TSL peaks. However, we cannot exclude also the direct ionization of some impurities with the release of electrons into the conduction band because, for example, the number of $(CrO_4)^{3-}$ centres decreases after irradiation by energy $h\nu < E_g$.

The complex TSL peak, located around 230 K, consisting of at least three components located at 226, 232 and 238 K and dominating in the as-grown sample, is assumed to arise from non-paramagnetic $\{WO_2\}$- and/or {WO}-related electron centres which appear under irradiation around 4.05 eV as a result of the decay of excitons of the type $(WO_4)^{2-}$ localized near oxygen vacancies of the type of WO_2(ex^0WO_2) and/or WO (ex^0WO). We assume that during photo-thermally stimulated decay of these excitons, the electrons and holes are released. Released electrons are trapped at/near the oxygen-deficient anion complexes of the WO_2 and/or WO type. It is not excluded that two electrons are trapped at the same complex, which could explain the fact that the electron centres responsible for the ≈230 K peak are not observed in the ESR spectra. The average value of the trap depth E_t is about 0.56 eV. The optically released holes are most probably trapped at the lead vacancy-related centres. As follows from the ESR data, thermal destruction of hole centres takes also place in this temperature range and can contribute to the observed TSL characteristics.

Weak TSL peaks at ≈305 and 340 K arise from the electron centres of the WO_3^- type localized near monovalent impurity ions or lead vacancies [21] (a small number of $\{WO_3^-–A^+\}$

or $\{WO_3^- – V_{Pb}\}$ centres were also detected in the ESR). Their creation spectra and E_a values are close to those of the ≈205 K peak (see figure 7 and table 3). The dependence of the TSL intensity on the irradiation temperature shown in figure 8 confirms the conclusion [21] that these centres appear at the thermal destruction of the optically created $\{Pb^+ – WO_3\}$ centres.

Under irradiation in the defect-related band (around 3.8 eV), some other centres responsible for the ≈230 K peak are created. Indeed, in this case the shape of the TSL peak and the corresponding trap depth E_t (figure 6) differ from those obtained under irradiation in the exciton region. The superlinear dose dependence presented in figure 5(b) for this peak indicates that free electrons can be released in this energy range [9, 16].

5. Conclusions

The results obtained in the present paper allow us to suggest that excitons of the type $(WO_4)^{2-}$ localized at oxygen-deficient anion complexes of different types (WO_3, WO_2, WO) exist in the $PbWO_4$ crystals studied. The photo-thermally stimulated decay of the localized excitons results in the creation of various oxygen vacancy-related electron centres as well as hole centres, most probably connected with lead vacancies. At $T < 295$ K, their thermally stimulated recombination is accompanied with the G(II) emission (2.5 eV).

The following processes are assumed to take place:

$$ex^0WO_3 \rightarrow \{Pb^+ – WO_3\}; ex^0WO_2 \rightarrow \{e^- \text{ or } 2e^- \text{ at/near } WO_2\}; ex^0WO \rightarrow \{e^- \text{ or } 2e^- \text{ at/near WO}\}.$$

The WO_3-related electron centres are probably responsible for the TSL peaks in the annealed sample located in the 170–205 K range. The TSL peak at approximately 205 K arises from the $\{Pb^+ – WO_3\}$-type centres created by the decay of ex^0WO_3 [4]. Thermal liberation of electrons from the WO_2- and/or WO-related electron traps and holes from unspecified hole traps can contribute to the complex TSL peak located around 230 K.

Strongly selective creation of various TSL peaks, as well as data on the decay kinetics of the tunnelling recombination G(II) emission obtained in [9] indicate that localized exciton decay takes place without the release of free electrons into the conduction band. Free electrons are optically created only at the decay of the STE and defect-related states.

Different TSL peaks appear (i) after trapping of free charge carriers by the traps existing in the crystal and (ii) after localized excitons decay into electron and hole centres. In the crystals studied, defects are most effectively created by the decay of localized excitons (at $T_{irr} > 130$ K) and due to the charge-transfer processes in close defect pairs (at $T_{irr} < 120$ K). The STE decay makes a comparatively smaller contribution to the defect creation process.

Acknowledgments

This work was partly supported by the Estonian Science Foundation grant no. 6548 and Czech Institutional Research Plan AV0Z10100521. Thanks are due to N Senguttuvan and M Ishii for growing the crystals used in this study.

References

[1] Lecoq P, Dafinei I, Auffray E, Schneegans M, Korzhik M V, Missevitch O V, Pavlenko V B, Fedorov A A, Annenkov A N, Kostylev V N and Ligun V D 1995 *Nucl. Instrum. Methods Phys. Res.* A **365** 291
[2] Nikl M 2000 *Phys. Status Solidi* a **178** 595
[3] Annenkov A A, Korzhik M V and Lecoq P 2002 *Nucl. Instrum. Methods Phys. Res.* A **490** 30

[4] Krasnikov A, Nikl M and Zazubovich S 2006 *Phys. Status Solidi* b **243** 1727
[5] Babin V, Bohacek P, Krasnikov A, Nikl M, Stolovits A and Zazubovich S 2007 *J. Lumin.* **124** 113
[6] Krasnikov A, Nikl M, Stolovits A, Usuki Y and Zazubovich S 2005 *Phys. Status Solidi* c **2** 77
[7] Babin V, Bohacek P, Bender E, Krasnikov A, Mihokova E, Nikl M, Senguttuvan N, Stolovits A, Usuki Y and Zazubovich S 2004 *Radiat. Meas.* **38** 533
[8] Groenink J A and Blasse G 1980 *J. Solid State Chem.* **32** 9
[9] Fabeni P, Kiisk V, Krasnikov A, Nikl M, Pazzi G P, Sildos I and Zazubovich S 2007 *Phys. Status Solidi* c **4** 918
[10] Korzhik M V, Pavlenko V B, Timoshenko T N, Katchanov V A, Singovskii A V, Annenkov A N, Ligun V A, Solski I M and Peigneux J-P 1996 *Phys. Status Solidi* a **154** 779
[11] Bohacek P, Senguttuvan N, Kiisk V, Krasnikov A, Nikl M, Sildos I, Usuki Y and Zazubovich S 2004 *Radiat. Meas.* **38** 623
[12] Mürk V, Nikl M, Mihokova E and Nitsch K 1997 *J. Phys.: Condens. Matter* **9** 249
[13] Bohacek P, Fabeni P, Krasnikov A, Nikl M, Pazzi G P, Susini C and Zazubovich S 2005 *Phys. Status Solidi* c **2** 547
[14] Bohacek P, Fabeni P, Krasnikov A, Nikl M, Pazzi G P, Susini C and Zazubovich S 2006 *Radiat. Prot. Dosim.* **119** 164
[15] Mihokova E, Nikl M, Bohacek P, Babin V, Krasnikov A, Stolovits A, Zazubovich S, Vedda A, Martini M and Grabowski T 2003 *J. Lumin.* **102/103** 618
[16] Laguta V V, Nikl M and Zazubovich S 2007 *Radiat. Meas.* doi:10.1016/j.radmeas.2007.01.044
[17] Senguttuvan N, Ishii M, Tanji K, Kittaka T, Usuki Y, Kobayashi M and Nikl M 2000 *Japan. J. Appl. Phys.* **39** 5134
[18] Laguta V V, Vedda A, Di Martino D, Martini M, Nikl M, Mihokova E, Rosa J and Usuki Y 2005 *Phys. Rev.* B **71** 235108
[19] Krasnikov A, Nikl M and Zazubovich S 2006 *Proc. 8th Int. Conf. on Inorganic Scintillators and their Use in Scientific and Industrial Applications (Ukraine)* ed A Gektin and B Grinyov, p 362
[20] Laguta V V, Martini M, Vedda A, Nikl M, Mihokova E, Bohacek P, Rosa J, Hofstaetter A, Meyer B K and Usuki Y 2001 *Phys. Rev.* B **64** 165102
[21] Laguta V V, Martini M, Vedda A, Rosetta E, Nikl M, Mihokova E, Rosa J and Usuki Y 2003 *Phys. Rev.* B **67** 205102